Charm baryons at finite temperature on anisotropic lattices

Ryan Bignell,[a,*] **Gert Aarts,**[a,b,c] **Chris Allton,**[a] **M. Naeem Anwar,**[a] **Timothy J. Burns**[a] **and Benjamin Jäger**[d]

[a]*Department of Physics, Swansea University, Swansea, SA2 8PP, United Kingdom*

[b]*European Centre for Theoretical Studies in Nuclear Physics and Related Areas (ECT*)*

[c]*Fondazione Bruno Kessler, Strada delle Tabarelle 286, 38123 Villazzano (TN), Italy*

[d]*CP3-Origins & Danish IAS, Department of Mathematics and Computer Science, University of Southern Denmark, 5230, Odense M, Denmark*

Singly, doubly and triply charmed baryons are investigated at multiple temperatures using the anisotropic FASTSUM "Generation 2L" ensembles. We discuss the temperature dependence of these baryons' spectra in both parity channels with a focus on the confining phase. To further qualify the behaviour of these states around the pseudocritical temperature, we investigate the effect of chiral symmetry restoration for light quarks. We find that an estimate of the pseudocritical temperature can still be found from positive and negative-parity charmed baryon correlators, even when parity doubling itself is not very evident (as expected).

---

*Speaker

1. Introduction

As the temperature increases, the confining hadronic phase of Quantum Chromodynamics (QCD) smoothly [1] deforms to a deconfining quark-gluon plasma (QGP). In this phase the lighter quarks are deconfined while the heavier charm and bottom quarks may remain bound until higher temperature. This transition is experimentally investigated in particle collider experiments such as the Large Hadron Collider [2–4] and the Relativistic Heavy Ion Collider [5].

Here we examine the charmed baryon spectrum through lattice QCD simulations. We vary the temperature by use of a series of anisotropic ensembles with different temporal extents. Anisotropic ensembles allow fine control of temperature and allow for a greater number of temporal data points at each temperature which is key for spectral studies. Charm baryons are of interest as the heavier charm quark is produced in relatively high proportions in heavy-ion collisions and the QGP exists long enough for the charm quarks to diffuse [6, 7] and contribute to the hadronisation process.

In particular we examine the masses of the states as a function of temperature. The extraction of baryon masses at high temperature becomes difficult due to both the reduced number of temporal points and the more fundamental question of whether the hadron is a bound state at these temperatures. The extracted baryon masses may be of interest to phenomenology [6].

As extracting baryon masses becomes difficult at the highest temperatures, we instead compare positive and negative parity channels [8–10] using the correlation functions directly, to investigate the effect of the restoration of chiral symmetry in the QGP. While parity doubling is not expected due to the large charm quark mass, we still note a clear change of behaviour, occurring around the thermal crossover temperature for singly and doubly charmed baryons.

2. Lattice setup

We calculate two-point correlation functions using standard baryon interpolating operators [13, 14] on the FASTSUM "Generation 2L" thermal ensembles [10, 12]. These span a wide range of temperatures using a fixed-scale anisotropic approach with a Wilson-clover fermion action and Symanzik-improved gauge action [15–18]. The pion mass is 239(1) MeV. Table 1 shows the details of these ensembles.

Excited state effects are reduced by the use of Gaussian smearing [19] at the source and the sink. The root-mean-square radius of the smearing profile is ∼ 6.1 lattice sites, an amount chosen such that the ground-state isolation for the zero temperature positive parity nucleon is good.

Table 1: The FASTSUM Generation 2L ensembles used in this work which have lattice size $32^3 \times N_\tau$ and temperature $T = 1/(a_\tau N_\tau)$. The spatial lattice spacing is $a_s = 0.1121\,(3)$ fm, renormalised anisotropy $\xi = a_s/a_\tau = 3.453(6)$ and the pion mass $m_\pi = 239(1)$ MeV [11]. We use ∼ 1000 configurations and eight (random) sources for a total of ∼ 8000 sources at each temperature. Full details of these ensembles may be found in Ref. [10, 12].

N_τ	128	64	56	48	40	36	32	28	24	20	16
T (MeV)	47	95	109	127	152	169	190	217	253	304	380
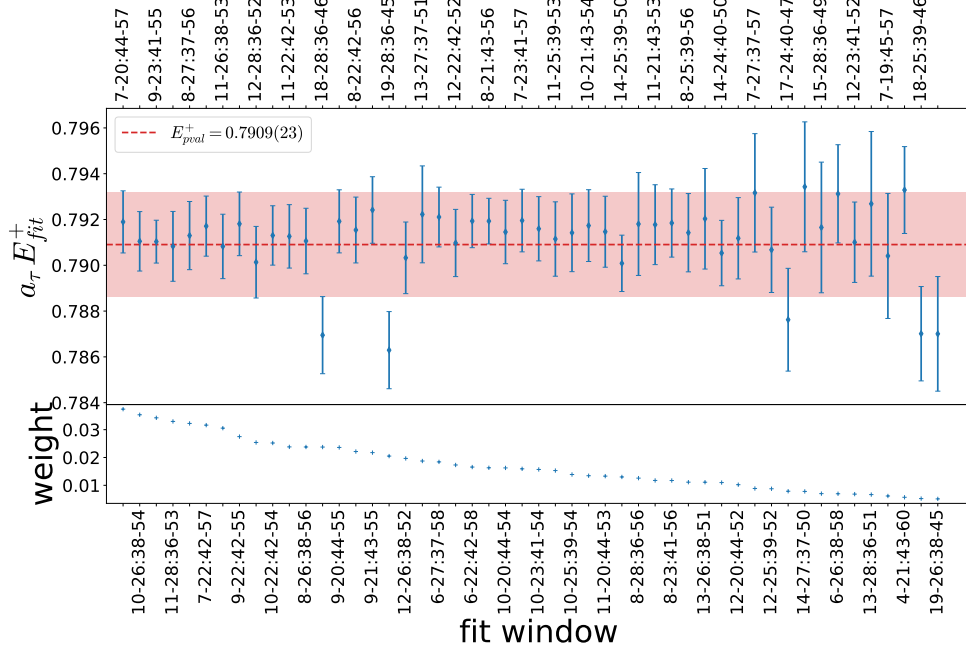
Figure 1: Highest weighted fit results for the $N_\tau = 64 \; \frac{3}{2} \Omega_{ccc}$ positive parity energy as a function of fit window. The weights of Ref. [22] are also shown, as is the resulting model averaged fit value. Both sides of the correlator are fit symmetrically e.g. "10-26:38-54" fits points $[10, 26]$ and $[38, 54]$ simultaneously.

3. Masses

The zero-momentum projected two-point correlation function has contributions from multiple positive and negative parity energy eigenstates. Accordingly, we fit the correlator using functions of the form

$$G\left(\tau\right) = \sum_{\alpha=1}^{N} A_\alpha e^{-a_\tau E_\alpha^+ \tau/a_\tau} + B_\alpha e^{-a_\tau E_\alpha^- (N_\tau - \tau/a_\tau)}, \tag{1}$$

where the number of exponentials is allowed to vary $N = 1, 2, 3$; E_α^+ are the positive parity energies and E_α^- are the negative parity energies. N is set by examination of the Gaussian Bayes factor [20, 21] which tells us that additional exponential terms would not increase the quality of the fit.

In order to ensure a robust determination of the masses, we make use of the model averaging methods presented in Refs. [22, 23]. Here all possible temporal subsets of the correlator ("fit-windows") are considered and the resulting fits are averaged with some weight. Outlying fits are excluded via a consideration of the 30% of fits with the highest weight from the Akaike information criterion weights [23]. The final mass is produced by picking the averaged result which most clearly represents the underlying fits. An example of this is shown in Figures 1 and 2 for the positive parity $N_\tau = 64 \; \frac{3}{2} \Omega_{ccc}$ state. In Figure 1 we show the highest weighted fits using the "p-value" method [22] where the fit-window is shown above and below. As we fit both sides of the correlator, the label reflects this. The averaged result encompasses the clear majority of fit weights and is not
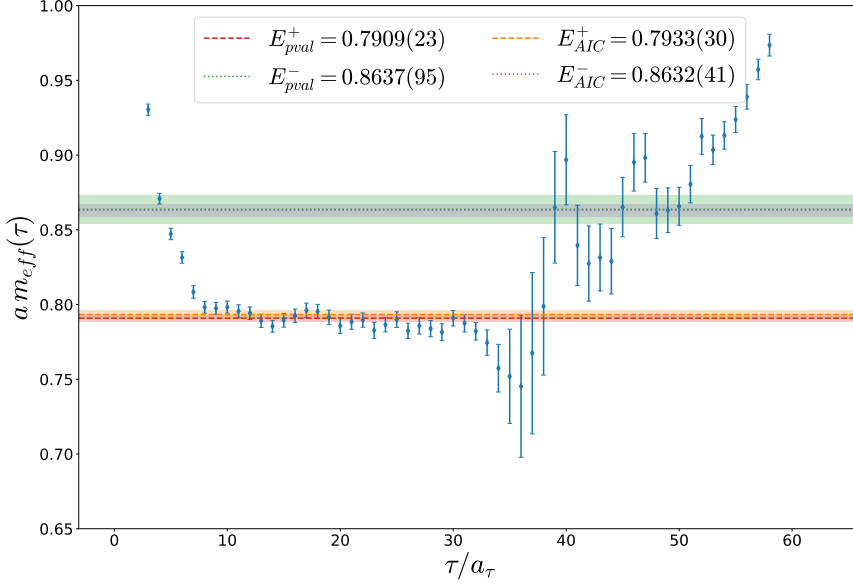
Figure 2: Effective mass for the $N_\tau = 64$ $\frac{3}{2}\Omega_{ccc}$ state showing the results of the two model averaging methods described in Refs. [22, 23].

an outlier or unstable result. A systematic uncertainty from the choice of averaging method is also considered.

A description of the charm baryon states investigated in this study is provided in Figure 3 which displays the ground-state charm baryon spectrum on the "zero temperature" $N_\tau = 128$ ensemble. The zero-temperature results are in good agreement with the experimental measurements for the states containing only s or c quarks as these quarks have been tuned to their physical values [24]. States containing u or d quarks are heavier than nature which is expected on these ensembles. The emphasis in this work is not on extreme precision zero-temperature spectroscopy [24, 25] and so Figure 3 is only a guide to the charmed baryons considered in this work.

We extend the analysis of Figure 3 to non-zero temperature for the $J = 1/2$ charmed baryons in Figure 4. Here the positive and negative parity sectors are shown separately, enabling an examination of the temperature dependence. It is clear that within each parity sector, different channels display qualitatively similar behaviour. Figure 4 suggests that the effect of temperature decreases with charmness C.

In Figure 5 a similar picture emerges for the $J = 3/2$ baryons. In this figure, the positive and negative parity plots do not share the same vertical scale however each subplot is the same. Here however the positive parity, $C = 3$ Ω_{ccc} mass is unaffected by temperature within uncertainties. This agrees with the pattern observed for the $J = 1/2$ sector where the $C = 1$ states displayed greater temperature dependence than the $C = 2$.

Determining the mass at non-zero temperature is a difficult task. This can be observed by the increasing uncertainty present in the preceding figures. The extracted masses suggest that above the transition temperature of ~ 167 MeV [29] the positive and negative parity sectors show greater temperature dependence. The suitability of the exponential ansatz of Eq. (1) at high temperatures
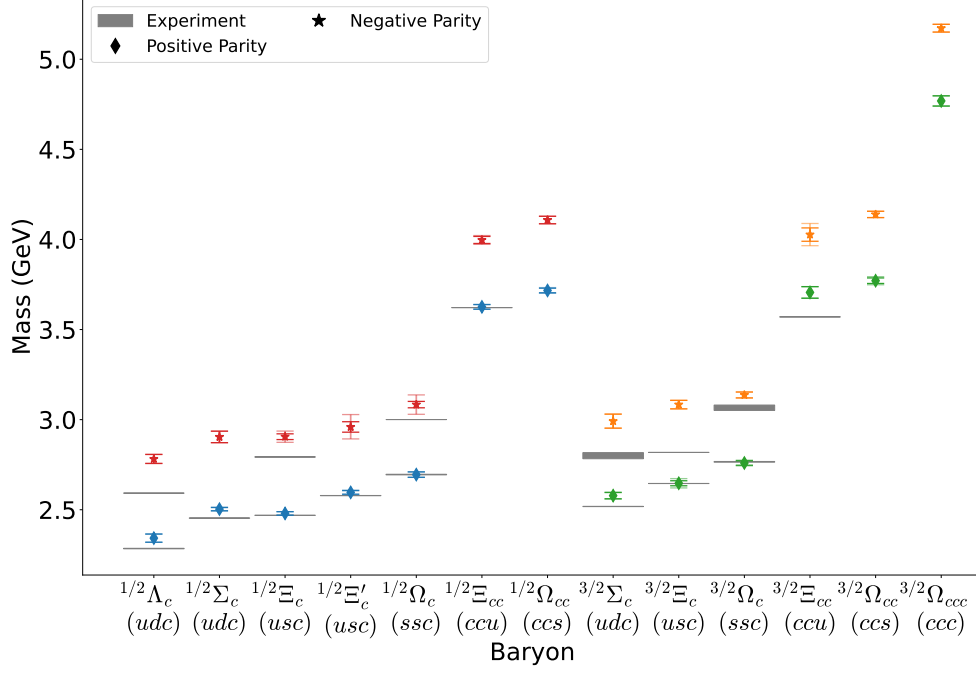
Figure 3: The ground-state charm baryon spectrum from the $N_t = 128$ zero-temperature ensemble. Positive parity states are shown by "diamonds" (♦) and the negative parity by "stars" (★). Inner error bars represent the statistical uncertainty and the outer incorporates a systematic from the choice of averaging method. The grey bands represent experimental results from the Particle Data Group [26] with uncertainties from different charge states added in quadrature. For the Ω_c we use the spin-parity assignments suggested in Refs. [27, 28]. We select $\Omega_c^{3/2-} = \Omega_c(3065)$ and include a systematic uncertainty encompassing the $\Omega_c(3050)$ mass due to the former's better known width.

is an interesting problem. Already at $N_\tau = 32$ ($T = 190$ MeV) the exponential fits do not seem to be describing all the states well. In particular the Ξ_{cc} is well described at this temperature, but not at the next hottest. The lighter states are ill-behaved at lower temperatures, which may be an indication they are no longer bound states at those temperatures. Nevertheless, we show the obtained masses, including the large uncertainty produced by our analysis - a sign of the breakdown of the ansatz. This problem could be better investigated with e.g. a spectral function function analysis or a correlator with more ground-state isolation before the interference of the positive and negative parity terms in the centre of the lattice. Such isolation could be achieved via a better determination of the correlator on these ensembles, or an ensemble with more temporal points at the same temperature. Both these methods are under investigation.

In summary, our results suggest that the temperature dependence is greater for negative parity states and in the $J = 3/2$ sectors.

4. Parity Doubling

Chiral symmetry is expected to-be restored in the QGP. For light and strange baryons, this results in a parity-doubling signal at the level of the correlators [8, 9]. For charmed baryons for
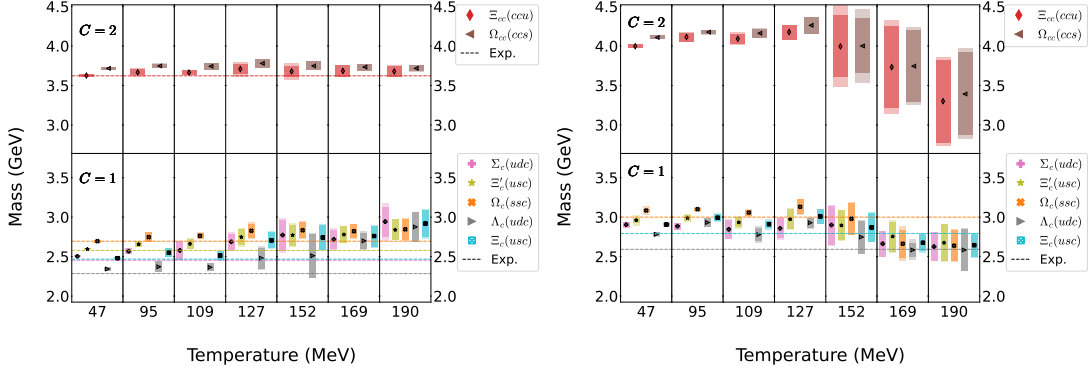
Figure 4: Left: Mass spectrum of $J^P = 1/2^+$ baryons as a function of temperature. Dashed lines are zero-temperature experimental results [26] to guide the eye. The inner shaded region represents the statistical uncertainty, and the outer incorporates the systematic from the choice of averaging method. The same vertical scale is used in each subplot, making comparison of the uncertainties possible. Some states have increasing uncertainties around and past T_{pc}. This may indicate these states becoming unbound at these temperatures. **Right:** Mass spectrum of $J^P = 1/2^-$ baryons.
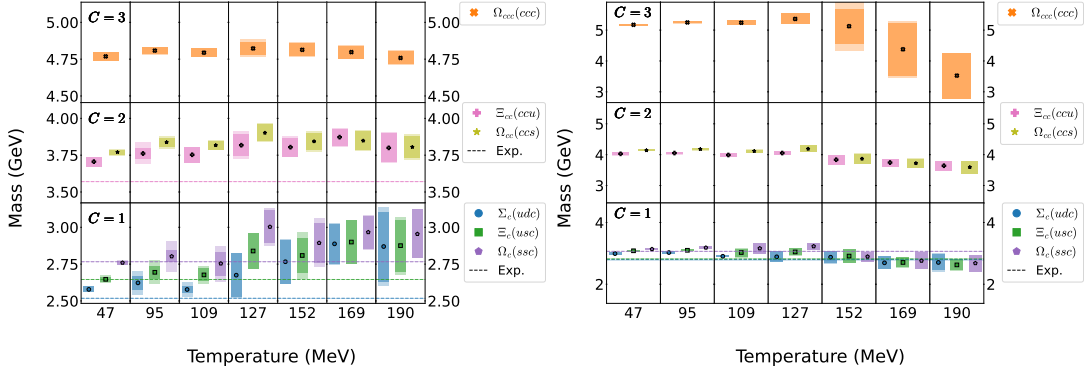
Figure 5: Left: Mass spectrum of $J^P = 3/2^+$ baryons as a function of temperature. Details as in Figure 4. **Right:** Mass spectrum of $J^P = 3/2^-$ baryons. Here positive and negative parity plots have different vertical scales.

the temperatures studied in this work, such a signal is not expected, since the charm quark mass breaks chiral symmetry explicitly. Nevertheless, it is interesting to study whether restoration of chiral symmetry for lighter quarks leads to visible effects in the charmed baryon sector.

We therefore turn to the parity doubling R-quantity considered in Refs. [30, 31]. This method has the advantage that no fits are required, enabling high statistical precision. We form the quantities

$$\mathcal{R}(\tau) = \frac{G^+(\tau) - G^-(\tau)}{G^+(\tau) + G^-(\tau)}, \tag{2}$$

$$R(n_0) = \frac{\sum_{n=n_0}^{\frac{1}{2}N_\tau - 1} \mathcal{R}(\tau_n)/\sigma_\mathcal{R}^2(\tau_n)}{\sum_{n=n_0}^{\frac{1}{2}N_\tau - 1} 1/\sigma_\mathcal{R}^2(\tau_n)}, \tag{3}$$

where $G(N_\tau a_t - \tau) = G^-(\tau)$ is the negative parity correlator, $G(\tau) = G^+(\tau)$ the positive parity correlator, and $\sigma_\mathcal{R}(\tau_n)$ denotes the statistical error for $\mathcal{R}(\tau_n)$. The sum over time slices
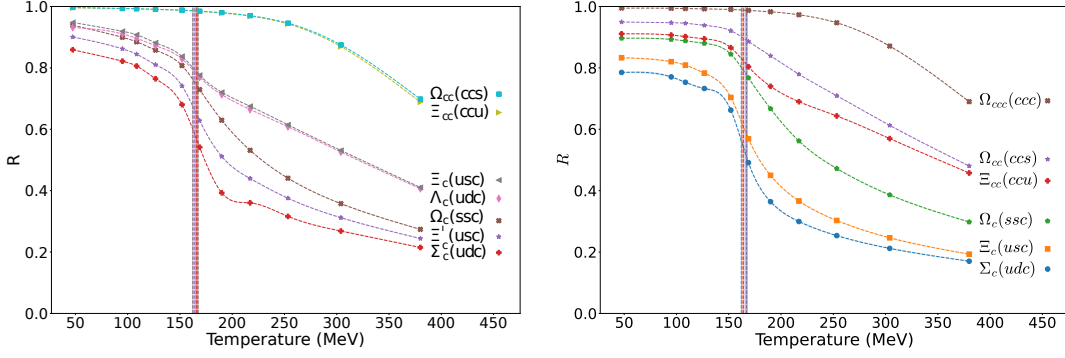
Figure 6: Left: R-quantity of Eq. (3) for $J = \frac{1}{2}$ baryons. The lines are cubic splines used to find the transition temperature which are shown in the vertical bands. **Right:** R-quantity of Eq. (3) for $J = \frac{3}{2}$ baryons.

$\tau_n \in [n_0 = 4, N_\tau/2 - 1]$ is chosen such that excited state contributions and lattice artefacts at small τ_n are suppressed. Small shifts in n_0 do not have a qualitative effect on the results.

As is clear from Eq. (2), $R \to 0$ when positive and negative correlators become degenerate, which coincides with chiral symmetry restoration. Conversely, when the states are non-degenerate with $m_+ \ll m_-$, R will be close to one. This is indeed the behaviour we see in Figure 6.

Due to the heavier mass of the charm quarks, chiral symmetry restoration is not expected, even at our highest temperatures. Again this is the effect seen in Figure 6 with it being particularly notable that the R-quantity increases monotonically with the number of charm quarks.

We also observe an intriguing similarity in the behaviour of the R-quantity for states (of a given J) which have the same charm content, and which belong to the same $SU(3)$ flavour multiplets, namely:

$$C = +2, \quad SU(3) \; \mathbf{3} : \quad \Omega_{cc}\,(ccs)\,, \; \Xi_{cc}\,(ccu)$$
$$C = +1, \quad SU(3) \; 3 : \quad \Lambda_c\,(udc)\,, \; \Xi_c\,(usc)$$
$$C = +1, \quad SU(3) \; \mathbf{6} : \quad \Sigma_c\,(udc)\,, \; \Xi'_c\,(usc)\,, \; \Omega_c\,(ssc)$$

A cubic spline interpolation of the data points for each hadron is performed; this enables the inflection point of the curves to be found. For singly-charmed baryons with $J = 1/2$ in Figure 6 left we find the inflection point to be near T_{pc}; interestingly, the doubly charmed $J = 1/2$ baryons do not have an inflection point. The ability of these inflection points to describe the transition temperature is present even when parity doubling is not nearly manifest, as for the $\Lambda_c(udc)$, as seen in Figure 6 left.

We repeat this exercise for the $J = 3/2$ baryons in Figure 6 right. Here we note that doubly charmed $J = 3/2$ baryons display an inflection point, again around T_{pc}. This is aligned with the results observed for masses, where the $J = 3/2$ states were more affected by temperature than the $J = 1/2$ states.

The inflection points found are presented in Figure 7 alongside the computation of the pseudo-critical temperature as obtained via the inflection point of the renormalised chiral condensate (blue band) [29]. Excellent precision and good agreement with the previous measurement is seen.
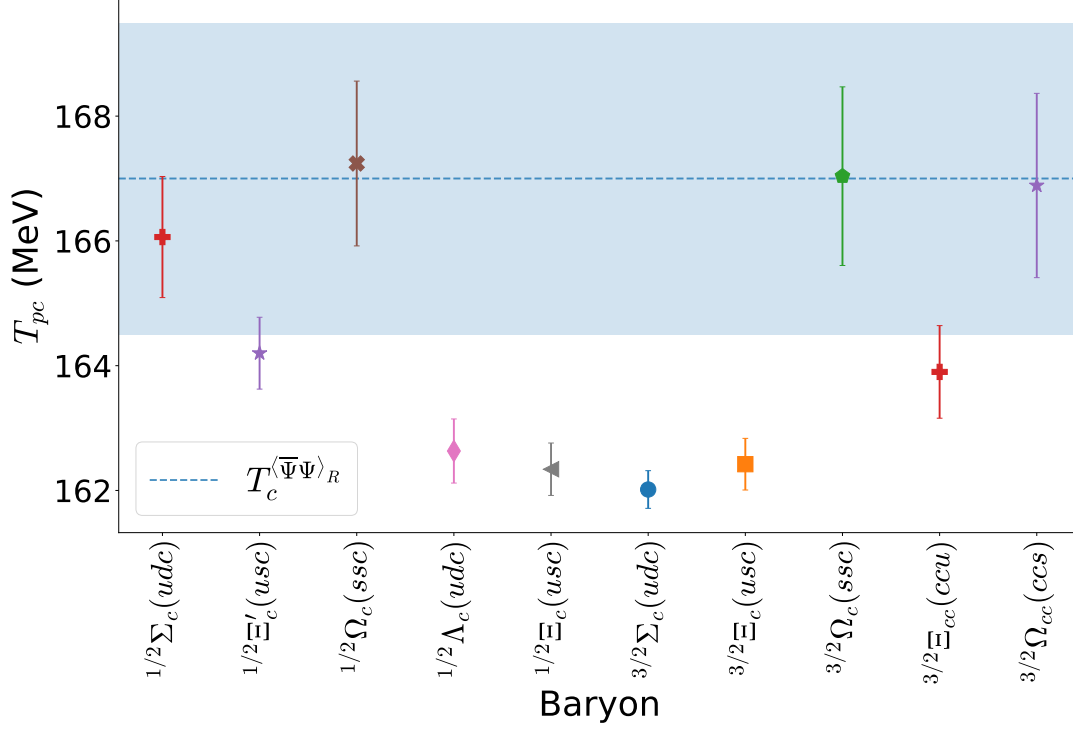
Figure 7: Inflection points of baryon *R*-quantity of Figure 6. The blue band is the pseudocritical temperature from the renormalised chiral condensate [29] adjusted for the change in lattice spacing [11, 12].

5. Conclusions & Future Work

A variety of singly, doubly and triply charmed baryons have been investigated using lattice QCD. We calculated two-point correlation functions at a range of temperatures using the FASTSUM "Generation 2L" anisotropic ensembles. Baryon masses were extracted by performing multi-exponential fits to all possible fit windows and considering two different methods with which to weigh the results. In the hadronic phase and just above the crossover, it is possible to extract ground state masses using the method described. At higher temperatures a more sophisticated spectral function analysis would be required.

To investigate the effect of chiral symmetry restoration, the correlator *R*-quantity was considered, to examine the difference between positive and negative parity correlation functions as a function of temperature. Despite the absence of parity doubling (due to the large charm quark mass), a crossover effect can nevertheless be observed, with inflection points close to the pseudocritical temperature.

In future work in preparation, we will examine more sophisticated methods of exploiting the correlators directly, as recently performed for the *D*-mesons in Ref. [12]. We anticipate providing the data and analysis tools at that time. In order to improve these results, one could construct a correlator which had more overlap with the ground-state or repeat the analysis on correlators with more temporal points at the same temperature.

Acknowledgments

References

[1] Y. Aoki, G. Endrodi, Z. Fodor, S. D. Katz and K. K. Szabo, *Nature* **443** (2006) 675–678, [`hep-lat/0611014`].

[2] N. Armesto and E. Scomparin, *Eur. Phys. J. Plus* **131** (2016) 52, [`arXiv:1511.02151`].

[3] W. Busza, K. Rajagopal and W. van der Schee, *Ann. Rev. Nucl. Part. Sci.* **68** (2018) 339–376, [`arXiv:1802.04801`].

[4] J. Berges, M. P. Heller, A. Mazeliauskas and R. Venugopalan, *Rev. Mod. Phys.* **93** (2021) 035003, [`arXiv:2005.12299`].

[5] P. Braun-Munzinger, V. Koch, T. Schäfer and J. Stachel, *Phys. Rept.* **621** (2016) 76–126, [`arXiv:1510.00442`].

[6] X. Yao and B. Müller, *Phys. Rev. D* **97** (2018) 074003, [`arXiv:1801.02652`].

[7] M. Begel et al., [`arXiv:2209.14872`].

[8] G. Aarts, C. Allton, D. De Boni, S. Hands, B. Jäger, C. Praki et al., *JHEP* **06** (2017) 034, [`arXiv:1703.09246`].

[9] G. Aarts, C. Allton, D. De Boni and B. Jäger, *Phys. Rev. D* **99** (2019) 074503, [`arXiv:1812.07393`].

[10] G. Aarts et al., *Phys. Rev. D* **105** (2022) 034504, [`arXiv:2007.04188`].

[11] D. J. Wilson, R. A. Briceno, J. J. Dudek, R. G. Edwards and C. E. Thomas, *Phys. Rev. Lett.* **123** (2019) 042002, [`arXiv:1904.03188`].

[12] G. Aarts, C. Allton, R. Bignell, T. J. Burns, S. C. García-Mascaraque, S. Hands et al., `arXiv:2209.14681`.

[13] D. B. Leinweber, W. Melnitchouk, D. G. Richards, A. G. Williams and J. M. Zanotti, *Lect. Notes Phys.* **663** (2005) 71–112, [`nucl-th/0406032`].

[14] SciDAC, LHPC, UKQCD collaboration, R. G. Edwards and B. Joo, *Nucl. Phys. B Proc. Suppl.* **140** (2005) 832, [`hep-lat/0409003`].

[15] R. G. Edwards, B. Joo and H.-W. Lin, *Phys. Rev. D* **78** (2008) 054501, [`arXiv:0803.3960`].

[16] B. Sheikholeslami and R. Wohlert, *Nucl. Phys.* **B259** (1985) 572.

[17] K. Symanzik, *Nucl. Phys.* **B226** (1983) 187–204.

[18] K. Symanzik, *Nucl. Phys.* **B226** (1983) 205–227.

[19] S. Gusken, *Nucl. Phys. Proc. Suppl.* **17** (1990) 361–364.

[20] G. P. Lepage, B. Clark, C. T. H. Davies, K. Hornbostel, P. B. Mackenzie, C. Morningstar et al., *Nucl. Phys. B Proc. Suppl.* **106** (2002) 12–20, [`hep-lat/0110175`].

[21] P. Lepage and C. Gohlke, Dec., 2021. 10.5281/zenodo.5777652.

[22] E. Rinaldi, S. Syritsyn, M. L. Wagman, M. I. Buchoff, C. Schroeder and J. Wasem, *Phys. Rev. D* **99** (2019) 074510, [`arXiv:1901.07519`].

[23] W. I. Jay and E. T. Neil, *Phys. Rev. D* **103** (2021) 114502, [`arXiv:2008.01069`].

[24] HADRON SPECTRUM collaboration, L. Liu, G. Moir, M. Peardon, S. M. Ryan, C. E. Thomas, P. Vilaseca et al., *JHEP* **07** (2012) 126, [`arXiv:1204.5425`].

[25] M. Padmanath, *PoS* **CHARM2020** (2021) 014, [`arXiv:2109.04748`].

[26] PARTICLE DATA GROUP collaboration, P. Zyla et al., *PTEP* **2020** (2020) 083C01.

[27] H.-Y. Cheng, *Chin. J. Phys.* **78** (2022) 324–362, [`arXiv:2109.01216`].

[28] H.-X. Chen, W. Chen, X. Liu, Y.-R. Liu and S.-L. Zhu, `arXiv:2204.02649`.

[29] G. Aarts et al., *PoS* **LATTICE2019** (2019) 075, [`arXiv:1912.09827`].

[30] S. Datta, S. Gupta, M. Padmanath, J. Maiti and N. Mathur, *JHEP* **02** (2013) 145, [`arXiv:1212.2927`].

[31] G. Aarts, C. Allton, S. Hands, B. Jäger, C. Praki and J.-I. Skullerud, *Phys. Rev. D* **92** (2015) 014503, [`arXiv:1502.03603`].

PoS(LATTICE2022)170